Research on Chemical Intermediates (2023) 49:5015–5028
https://doi.org/10.1007/s11164-023-05117-0

Effects of MgO on Ni/Al_2O_3 catalysts for CO_2 reforming of methane to syngas

Yousef A. Al-Baqmaa[1] · Ahmed S. Al-Fatesh[1] · Ahmed A. Ibrahim[1] · Abdulaziz A. Bagabas[2] · Fahad S. Almubadde[1] · Abdulaziz I. Alromaeh[2] · Jehad K. Abu-Dahrieh[3] · Ahmed E. Abasaeed[1] · Anis H. Fakeeha[1]

Received: 11 June 2023 / Accepted: 18 August 2023 / Published online: 15 September 2023

Abstract

Carbon dioxide reforming of methane (CRM) converts CH_4 and CO_2 greenhouse gases into syngas over nickel-based catalysts. We performed CRM in a tubular microreactor at 700 °C by using 5.0 wt.% NiO catalyst, supported over mixtures of γ-$Al_2O_3 + x$ MgO ($x = 20$, 30, 63, and 70 wt.%). The process of impregnation was used to prepare the catalysts. For characterization, N_2-physisorption, XRD, H_2-TPR, TGA, and Raman spectroscopy techniques were employed. Among the examined catalysts, $5Ni/Al_2O_3 + 63\%MgO$ was found the most active, where it showed ≅ 72% CH_4 conversion, 73% CO_2 conversion, and 0.82 H_2/CO mole ratio over 7 h of reaction. The MgO modifier was the primary component, which favorably affected both Ni dispersion and stability, for the good interaction between NiO and γ-alumina. The mono-supported samples displayed the lowest total hydrogen consumption. In TGA, the $5Ni/Al_2O_3 + 63\%MgO$ exhibited a significant weight decrease (40%), reflecting its activity. Furthermore, the Raman spectroscopy analysis showed that the crystallinity of the carbon over this catalyst was more pronounced than the others.

Keywords Carbon dioxide reforming of methane · Ni-based catalyst · MgO modifier · γ-Al_2O_3 support

Introduction

In recent years, the CRM has attracted considerable interest in the production of H_2 and CO combination known as synthesis gas. This gas, with its component gases in a mole ratio close to one, is appropriate for the Fischer–Tropsch method and the creation of methanol. In addition, CRM offers a great chance for a clean environment by utilizing the greenhouse gases (GHGs): carbon dioxide and methane [1–7]. Because it allows chemical reactions to be carried out at low temperatures without increasing or causing the production of byproducts, heterogeneous catalysis is a crucial

Extended author information available on the last page of the article

pillar for research on energy and its sustainability [8–13]. It has been demonstrated that heterogeneous catalysts based on transition metals are effective for producing fine and bulk compounds as well as hydrogenating petroleum. Click or tap here to enter text [14]. To find affordable, widely available hydrogenation catalysts, research has been focused on non-precious metals. Transitional metals like iron (Fe), cobalt (Co), and nickel (Ni) have drawn a lot of interest due to their unique characteristics, which include their enormous availability, low cost, lack of toxicity, and remarkable catalytic activities [14–17]. CRM is an environmentally friendly, economically feasible reaction for the conversion of CH_4 and CO_2 into syngas. Despite spending less time in the atmosphere than carbon dioxide, methane has a stronger warming effect. Since hydrogen is a necessary component of all petrochemical industries and renewable energy sources, the usage of GHGs in the course of the reforming tasks results in their conversion to H_2, which lessens the environmental impact of emitted GHGs on the atmosphere. CRM, steam reforming of methane, and partial oxidation are well-researched methods for the creation of syngas:

$$CH_{4(gas)} + CO_{2(gas)} = 2H_{2(gas)} + 2CO_{(gas)} \Delta H_{298} = 261 \text{ kJ mol}^{-1} \text{ CRM} \quad (1)$$

$$CH_{4(gas)} + H_2O_{(gas)} = 3H_{2(gas)} + CO_{(gas)} \Delta H_{298} = 206 \text{ kJ mol}^{-1} \text{ Steam reforming} \quad (2)$$

$$CH_{4(gas)} + \frac{1}{2}O_{2(gas)} = 2H_{2(gas)} + CO_{(gas)} \Delta H_{298} = -36 \text{ kJ mol}^{-1} \text{ Partial oxidation} \quad (3)$$

The H_2/CO mole ratio from CRM is superior to traditional steam reforming for the Fischer–Tropsch process and methanol synthesis [18]. In addition to having the lowest running costs of these processes, CRM also has the added advantage of converting CO_2 into useful chemicals [19].

Among the side reactions, the reverse water–gas shift (RWGS) is crucial for decreasing the H_2/CO mole ratio:

$$H_2 + CO_2 \leftrightarrow H_2O + CO \quad \Delta H^{o} = 42.1 \text{ kJ mol}^{-1} \quad (4)$$

The fast catalyst deactivation by carbon deposition and the high-temperature sintering of both the support and the active metal particles are disadvantages of dry reforming processes [20]. (Alumina (Al_2O_3) has frequently been used as catalyst support. However, a number of other support materials, including MgO, ZrO_2, La_2O_3, TiO_2, SiO_2, and ZrO_2-Al_2O_3, have been tested. There is consensus in the literature about the critical role of support materials in the CRM process [21–24]. Because of its mechanical strength, stability at high temperatures, and advantageous textural properties, alumina is frequently chosen for use as a support [25]. However, alumina-supported nickel-based catalysts are vulnerable to carbon deposition. [26]. Recent research has found that NiO/MgO or NiO/Al_2O_3 catalysts, in which NiO creates a solid solution with the support (NiO–MgO or $NiAl_2O_4$), inhibit carbon deposition [27–30]. In addition, it was noted that the basicity of MgO with other oxides, when used as a support, reduced carbon deposition and increased catalyst stability.

The dry reforming of biogas on a Ni catalyst supported on ZrO_2 and its modification with La_2O_3 and CeO_2 were both studied by Charisiou et al. [31]. According to their findings, modified support catalysts had better conversion rates and less performance degradation during prolonged reactions. In their study, Siahvashi and Adesina [32] investigated the carbon buildup that occurs during the CO_2 reforming reaction of C_3H_8 over alumina-supported bimetallic Mo/Co–Ni catalysts. The results showed that the reaction rate profiles of the Mo–Ni catalyst had higher H_2/CO formation rates with a lower CO_2 consumption rate compared to the Co–Ni catalyst. Additionally, the conversion-time analysis indicated that the Mo–Ni catalyst was more stable and active during a 72-h run, while the Co–Ni catalyst experienced noticeable deactivation after only 30 h on-stream. Cui et al. [33] investigated the Ni_3Co (1 1) coke behavior and reaction process using density functional theory. It was discovered that Ni and Co have an electrical synergistic effect that keeps Ni active even after carbon buildup, and the Ni_3Co (1 1) catalyst enhances O* transport properties and lowers the energy barrier for C–O bonding. As a result, carbon deposition can be prevented.

Foo and colleagues [34] looked into the kinetics of carbon deposition and removal on lanthanide-promoted Co–Ni/Al_2O_3 dry reforming catalysts. As a result of the rare-earth oxide interacting with the more reactive surface carbonaceous materials in redox reactions decreased coke accumulation. Using Ni catalysts supported on La_2O_3-Sm_2O_3-CeO_2, La_2O_3-Pr_2O_3-CeO_2, and La_2O_3-MgO-CeO_2, Siakavelas et al. [35] examined the CO_2 methanation process. It was established that a greater population of oxygen vacant sites was produced when La^{3+}, Pr^{3+} and La^{3+}, Sm^{3+} were simultaneously incorporated into the crystal structure of cerium oxide. Additionally, a large number of moderate basic sites was raised by the coexistence of La^{3+}, Mg^{2+} and La^{3+}, Pr^{3+} in CeO_2. The pace of the CO_2 methanation reaction was accelerated by these physicochemical characteristics at very low temperatures. Therefore, we impregnated NiO into commercially available combinations of MgO-modified Al_2O_3 of different MgO loadings. We denoted them by the letters 5Ni-MG*x*, where *x* (*x* = 20, 30, 63, and 70%) denotes the weight loading of MgO in the support. These 5Ni-MG*x* catalysts were characterized by N_2-physisorption, XRD, TPR, and TEM, and were tested in CRM at 700 °C. The effect of the loading of the MgO modifier on the catalyst activity and stability was studied.

Experimental

Catalyst preparation

To prepare 5Ni-MG*x*, *x* = (20, 30, 63, and 70%), 20 mL of distilled water, and the appropriate amount of nickel nitrate hexahydrate [Ni $(NO_3)_2.6H_2O$, 98%, Alfa Aesar] to get 5.0 wt.% loading of nickel oxide, and the required amount of support (the supports with different alumina and magnesium oxide ratios were obtained as a gift from SASOL Anckelmannsplatz 1, 20537, Hamburg, Germany) were mixed and were stirred at room temperature in a crucible. For 30 min, the solution was dried while being stirred at 80 °C. The catalysts were calcined at 700 °C for 3 h.

Catalytic testing

An amount of 0.1 g of catalyst was used to evaluate the activity in a fixed-bed, continuous-flow reactor (9.0 mm i.d. and 300 mm in length) at 1.0 atm. To show the reaction temperature, a thermocouple was attached in the center of the catalyst bed. The catalysts were pretreated by adding H_2 at a flow rate of 30 mL/min for one hour at 800 °C. To remove any remaining H_2 in the reactor, it was then purged with flowing N_2 at a rate of 20 mL/min for 20 min at 700 °C. During the reaction, the reactant feed gas $CH_4/CO_2/N_2$ with a volume ratio of 30/30/10 was injected and kept flowing at a rate of 70 mL/min, at a space velocity of 42,000 mL/(hg_{cat}), and at a temperature of 700 °C. A thermal conductivity detector (TCD)-equipped online GC (GC-Shimadzu 2014) was used to quantitatively assess the reaction products and unconverted feed gases from the reactor.

Catalyst characterization

Nitrogen physisorption at − 196 °C was used to measure the specific surface area of catalysts. The specific surface area was measured using a Micromeritics Tristar II 3020 device using the Brunauer–Emmett–Teller (BET) method. With the aid of a Shimadzu TGA-51 and thermal gravimetric analysis performed in the air, the amount of carbon deposition on the used catalysts was measured. The type of carbon deposited over the employed catalysts, along with the degree of graphitization, was determined using a laser Raman spectrometer (JASCO NRS-4500, Tokyo, Japan). The excitation beam employed had a wavelength of 532 nm. Using a transmission electron microscope (JEM-2100 F JEOL, Akishimashi, Tokyo, Japan), the morphology of the used catalysts was studied. An X-ray diffractometer (Miniflex Rigaku diffractometer), outfitted with Cu K X-ray radiation and operating at 40 kV and 40 mA, was used to investigate the crystalline phases of the fresh catalysts. Data collection took place over a 2-h period with a step magnitude of 0.01° and a 2- angle range of 10–85°. A Micromeritics Auto-Chem II 2920 device was used to perform H_2 temperature-programmed reduction (H_2-TPR). The catalyst sample was heated for one hour at 200 °C in an argon environment before to the measurements, and it was then cooled to room temperature. Using a gas mixture of H_2/Ar (v/v, 10/90) at a flow rate of 40 mL/min, 0.07 g of the sample was heated at a rate of 10 °C/min to 1000 °C. Using a TCD, the H_2 consumption signal was captured.

Results and discussion

Figure 1A shows the N_2 adsorption–desorption isotherms of the fresh catalysts. According to IUPAC classification [36], the isotherms have H3 hysteresis loops and are of type-IV. These patterns are traits of mesoporous materials and often apply to solid particles with wedge, plate slit, and crack structures [36]. Figure 1 demonstrates, however, that N_2 uptake increased in the 0.5–1 relative pressure range (P/

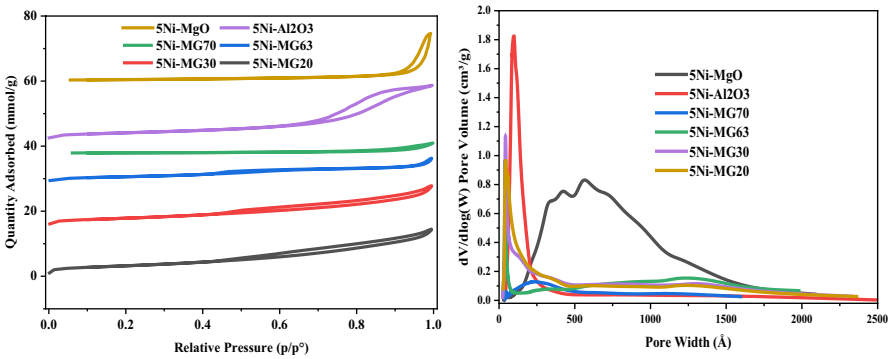

Fig. 1 N_2 adsorption–desorption isotherms of the fresh catalysts and their BJH pore size distribution, based on adsorption isotherms

P0). The 5Ni-MG20 catalyst had the maximum surface area (260.2 m^2/g), whereas the 5Ni-MG70 catalyst had the lowest surface area (16.8 m^2/g) (Table 1). Results from tests of surface area and porosity revealed that the catalysts were mesopores. The reduction in the specific surface area and pore volume with increasing the weight percentage loading of the MgO modifier might be due to the blockage of pores by the modifier. In addition, all the modified catalysts, except 5Ni-Mg70, have higher surface area than the unmodified catalysts.

Figure 1B displays the BJH pore size distributions, based on the adsorption isotherms, of the fresh catalysts. The 5Ni-Al_2O_3 catalyst showed monomodal pore size distribution within the micro-mesoporous range with the highest pore volume of 0.52 cm^3/g. When MgO modifier was incorporated, multimodal distribution with spanning the micro-meso-macroporous range, associated with the reduction in pore volume from 0.512 to 0.105 cm^3/g with increasing MgO wt.% content from 20 to 70. This reduction in pore volume could be attributed to the blockage of pores and

Table 1 N_2-physisorption results of the fresh catalysts

Catalyst denotations*	Surface area (m^2/g)	Pore volume (cm^3/g)	Pore size (Å)
5Ni-MG20	260	0.512	78.5
5Ni-MG30	230	0.455	79.3
5Ni-MG63	175	0.268	67.9
5Ni-MG70	17	0.105	227.3
5Ni-Al_2O_3	173	0.520	12.8
5Ni-MgO	37	0.350	423.2

*5Ni-MG20 = 5%Ni/20%Mg-80% Al_2O_3; 5Ni-MG30 = 5%Ni/30%Mg-80% Al_2O_3

5Ni-MG63 = 5%Ni/63%Mg-80% Al_2O_3; 5Ni-MG70 = 5%Ni/70%Mg-80% Al_2O_3

5Ni-Al2O3 = 5%Ni/γ-Al_2O_3; 5Ni-Mg = 5%Ni/Mg

to the increase of pore width with increasing MgO content. The 5Ni-MgO catalysts showed also multimodal pore size distribution over the micro-meso-macroporous range, associated with pore volume of 0.35 cm^3/g.

To understand the interaction between the active catalyst and its support, H_2-TPR was carried out (Fig. 2). All the catalyst samples showed broad negative peaks in the temperature range of 50–600 °C, which could be attributed to the hydrogen spillover into the mesopores [31]. Furthermore, 5Ni-MG20 and 5Ni-MG30 catalysts retained some hydrogen in their pores until they reached 700 °C, while 5Ni-MG63 and 5Ni-MG70 catalysts had complete removal of hydrogen from their pores at 600 °C and showed onsets of positive peaks for the beginning of Ni^{2+} ions reduction. This observation indicated that increasing MgO content strengthened the interaction of NiO with the support, as reported previously in the literature [37]. All of the catalysts showed a broad peak of reduction in the 700–1000 °C region, indicating a strong interaction of NiO with the support. The peak's maximum, intensity, and broadness were all dependent on the amount of MgO present in the catalyst. The reduction peaks of 5Ni-MG20 and 5Ni-MG30 catalysts had similar maximums (~ 830 °C) and broadness, but the peak of 5Ni-MG30 had higher intensity than that of 5Ni-MG20, reflecting the effect of the higher MgO content. When MgO content increased to 63 wt.% (5Ni-MG63), the reduction peak maximum shifted to ~ 860 °C, its broadness increased, and its intensity reduced a little bit in comparison to that of 5Ni-MG30. Further increase of MgO content to 70 wt.% (5Ni-MG70) resulted in shifting the reduction peak maximum to ~ 930 °C, broadening the peak, and decreasing its intensity (the lowest peak intensity). Therefore, the successive increase in MgO content developed stronger interaction between NiO with the support. Such interaction could be attributed to the formation of $NiAl_2O_4$ spinel [32], Mg_2NiO_3 [33], $MgNi_2O_3$ [33], and $Ni_xMg_{(1-x)}$ O [34], where the letter three phases formed owing to the solid solution between NiO and MgO. Table 2 displays the amount

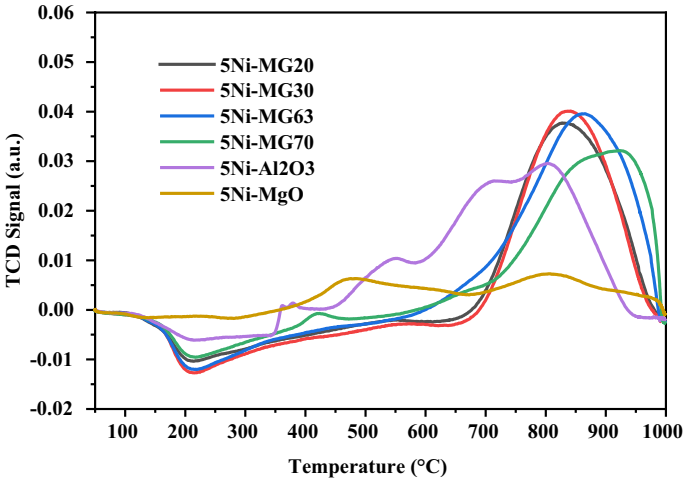

Fig. 2 H_2-TPR curves of the fresh catalysts

Table 2 The Analysis of H_2-consumption during H_2-TPR

Sample	Peak temperature (°C)	Quantity of H_2-consumption (cm^3/gSTP)	Total amount of H_2-consumption (cm^3/gSTP)
5Ni-Al_2O_3	379.2967	0.0634	25.9328
	534.6931	0.8812	
	695.2565	1.6031	
	802.7151	23.3851	
5Ni-MgO	483.5249	4.5348	11.1087
	803.8240	6.1401	
	990.6808	0.4338	
5Ni-MG20	125.1277	0.0027	24.0726
	209.9566	2.4175	
	541.1938	0.1012	
	829.6652	21.5731	
5Ni-MG30	210.9635	2.9236	24.5941
	545.4515	0.0958	
	841.0082	21.5754	
5Ni-MG63	212.3479	3.7289	31.55921
	861.3353	27.8301	
5Ni-MG70	210.6436	2.159559	29.7618
	419.2967	0.243732	
	924.5811	27.35911	

of hydrogen consumption during the TPR analysis of the catalysts. The 5Ni-Al_2O_3 catalyst showed a broad reduction peak between 700 and 1000 °C, centered at ~ 830 °C. The development of the $NiAl_2O_4$ spinel phase and the strong interaction of NiO with the Al_2O_3 support may be responsible for the high temperature of reduction. On the other hand, 5Ni-MgO catalyst did not show any reduction peak within the examined temperature range, implying the very strong interaction between NiO and MgO and the formation of solid solution and mixed metal oxides. 5Ni-MG63 showed the highest amount of hydrogen consumption, while 5Ni-MgO catalyst exhibited the lowest amount of hydrogen consumption. These results were in parallel with the observed catalytic performance.

The population of the basic sites of the reduced samples obtained from CO_2-TPD is inserted in the support information as Table S1.

Figure 3 displays the X-ray diffraction patterns of the fresh 5Ni-MGx ($x = 20$, 30, 63, or 70 wt.%) catalysts. The 5Ni-MGx catalysts' XRD patterns revealed diffraction peaks at 2θ of 35°, 46°, and 67°, which could be attributed, respectively, to (110), (113), and (214) crystallographic planes of the cubic γ-alumina phase (JCPDS No. 42-1468). In addition, the cubic phase of magnesium oxide was detected at 2θ of ~ 37°, 74°, and 78°, corresponding, respectively, to the crystallographic planes of (111), (311), and (222) (JCPDS card number 89-7746). The diffraction of MgO became obvious with the increase of its content in the catalyst. The diffraction peaks

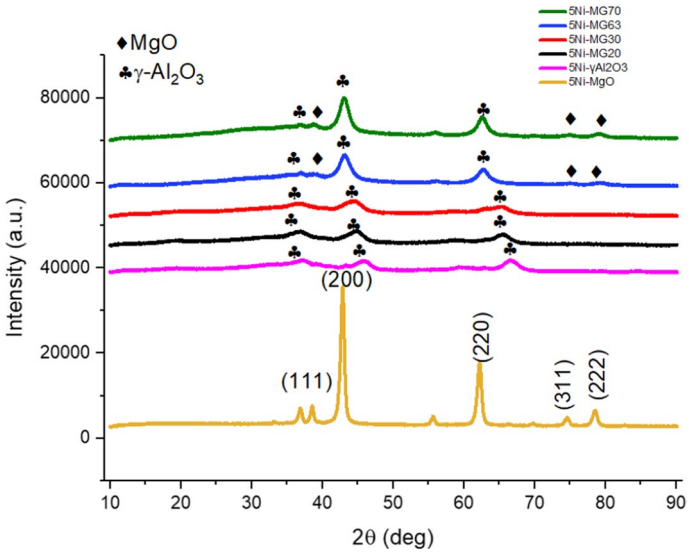

Fig. 3 XRD patterns of the fresh catalysts

of MgO could also be attributed to NiO (JCPDS Card No. 00-004-0835) because both of these oxides have the same crystal structure and form solid solutions [38].

In the course of catalytic performance, the same input ratio and reaction temperature of 700 °C were used in a stainless-steel reactor without catalysts, as part of a blank experiment before the evaluation of the synthesized catalysts. The blank's CH_4 and CO_2 conversions were 1.55 and 0.25%, respectively, the smallest influence of the metallic reactor is indicated by an H_2/CO mole ratio that is close to 0.11. Figure 4 shows the profiles of the CH_4 and CO_2 conversions as well as the H_2/CO ratio. Each 5Ni-MG*x* catalyst's performance ($x = 20$, 30, 63, or 70%) was evaluated at 700 °C. The 5Ni-MG30 catalyst gave the CH_4 conversion higher than the CO_2 conversion. This result might be attributed to the occurrence of methane cracking. The 5Ni-MG63 catalyst exhibited the optimal CRM performance, with CH_4 and CO_2 conversions of 72.9 and 72.3%, respectively, and an H_2/CO ratio of 0.82. Generally, the modification of alumina support with MgO reduces the generation of carbon deposit and improves the activity. The activity of 5Ni-MG63 was better than both 5Ni-MgO and 5Ni-Al_2O_3. The superb activity of 5Ni-MG63 could be related to its highest value of hydrogen consumption during the TPR. The higher the hydrogen consumption is, the higher the reduction of the active metal is.

Additional proof on the level of graphitization and the type of carbon on the used catalysts is provided by Raman spectroscopy. Comparative catalytic performances in relation to CH_4 and CO_2 conversions of other nickel-based catalysts with the current study are displayed in the support information (Table S2). A satisfactory resemblance is achieved.

The Raman spectra of the used catalysts are shown in Fig. 5. There were two zones in the spectra. Zone I ranged from 1250 to 1650 cm1, and Zone II ranged

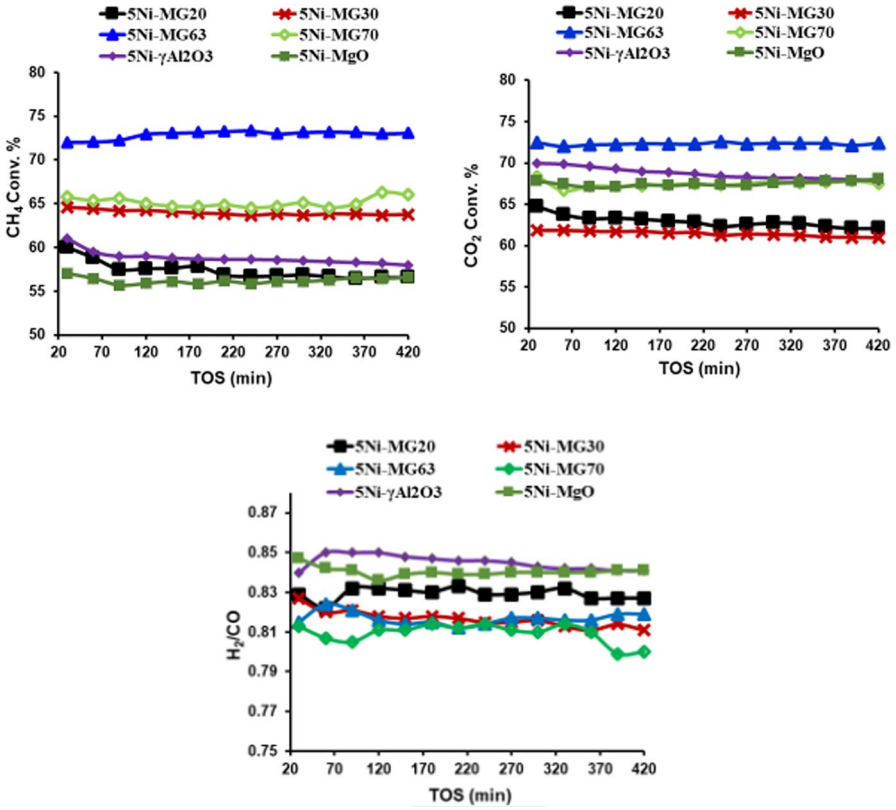

Fig. 4 Conversions of CH_4 and CO_2, and H_2/CO mole ratio as a function of TOS (reaction conditions: $CH_4/CO_2/N_2 = 3/3/1$ (v/v/v); GHSV = 42,000 ml/g_{cat}/h; $M_{cat} = 0.1$ g; $t = 700$ °C)

from 2400 to 3000 cm1. The D- and G-band characteristic peaks were located at 1343 and 1591 cm^{-1}, respectively, in zone I. The D-band is associated with defective, disorganized carbon deposits (amorphous), whereas the G-band is associated with graphite. The 2D band was seen at 2669 cm^{-1} as a result of the band of zone I's unification and ramifications. The relative intensity sizes of the G and D bands (ID/IG) allow for an accurate assessment of the degree of carbon crystallinity that was created during the reaction. Minor ratios indicate that crystallinity is predominant due to the graphitized carbon. For our spent catalysts, the values of I_D/I_G were 1.15, 1.04, 1.01, and 1.12 for the 5Ni-MG20, 5Ni-MG30, 5Ni-MG63, and 5Ni-MG70, respectively. The highest (ID/IG) ratios were seen in the 5Ni-MG20 and 5Ni-MG70 catalysts, which indicate low crystallinity as a result of a lack of graphitized carbon. As a result, compared to the other catalysts, the graphitization degree of the carbon over the 5Ni-MG20 and 5Ni-MG70 catalysts was evidently lower. The deposits of poor crystalline or amorphous carbon caused the early deactivation of the catalyst, while the crystalline graphitic carbon led to enhanced catalytic performance.

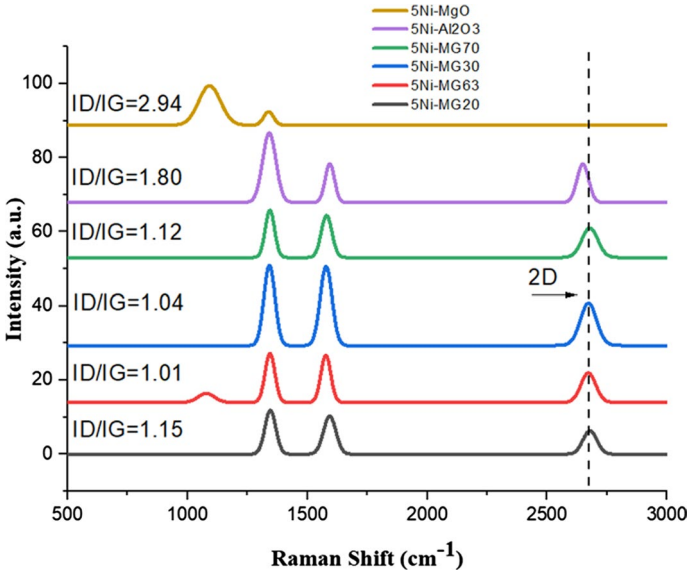

Fig. 5 Raman spectra of the spent catalysts

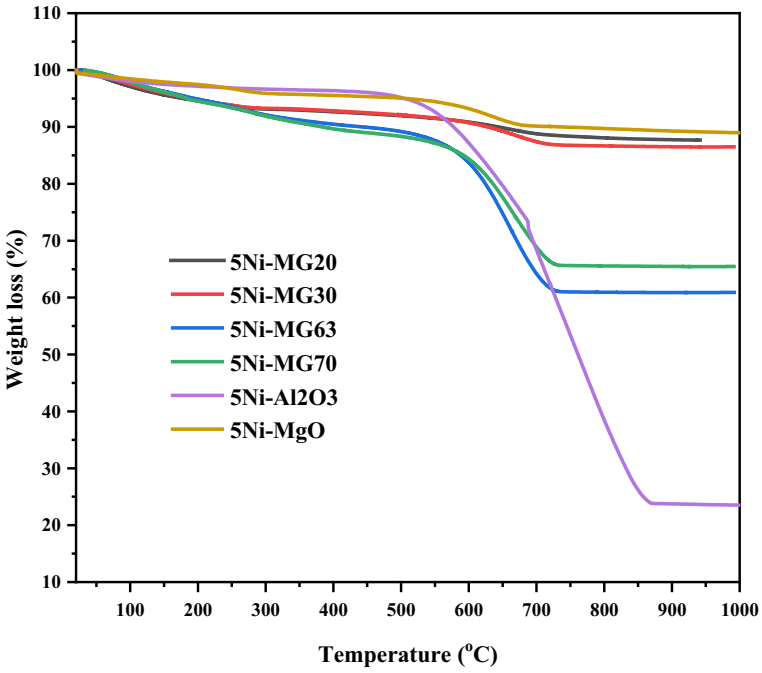

Fig. 6 TGA curves for the spent catalysts after 7 h time-on-stream

Figure 6 shows the weight loss of used catalysts as a function of temperature. The weight loss below 200 °C was primarily due to the elimination of H_2O and other chemisorbed species, whereas the weight loss between 200 and 500 °C was primarily brought about by the oxidation of amorphous carbon. The combustion of graphite carbon over 600 °C was the key factor, contributing to the weight loss. As shown in Fig. 6, the 5Ni-MG20 catalyst had a weight loss of 13%, while the 5Ni-MG63 had a high weight loss of 39%. This profile could be attributed to the reactivity of the catalysts. The 5Ni-MG20 exhibited low performance and thus generated low carbon deposition. On the other hand, 5Ni-MG63 catalyst showed high activity and hence generated a substantial amount of carbon deposition. The catalyst supported by unmodified Al_2O_3 with MgO gave the highest weight loss of 77%, which denoted that the modification of the support with MgO addition diminished the carbon formation.

The TEM images of 5Ni-MG*x* catalysts ($x = 30$ and 63%) at a 100 nm scale are shown in Fig. 7. Fresh and used 5Ni-MG30 catalysts are shown in Fig. 7A and B, respectively. Filamentous carbon nanotube production was visible in the catalytic waste. Figure 7C and D is for the fresh and spent 5Ni-MG63 catalysts, respectively, where the agglomerated catalyst particles were observed for the fresh 5Ni-MG63 catalyst and numerous filamentous carbon nanotubes for the spent one, respectively.

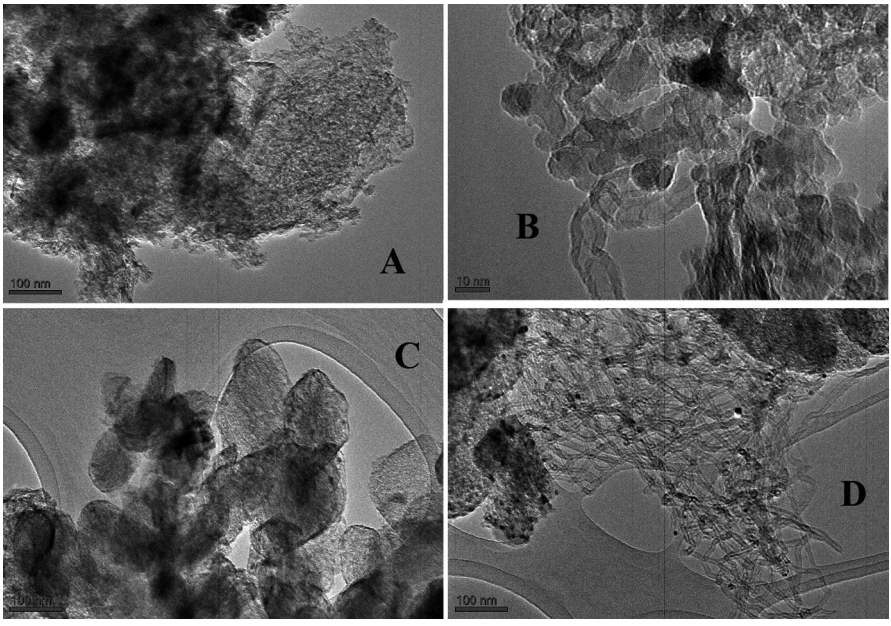

Fig. 7 TEM images of 5Ni-MG*x* ($x = 30$ or 63%) spent catalysts

Conclusions

Ni-based catalysts, supported on alumina-modified with MgO, generated syngas through CO_2 reforming of methane (CRM). The catalytic activity for CRM increased with the increasing MgO modifier loading. 72% CH_4 conversion and 73% CO_2 conversion over 7-h time-on-stream were obtained when 63% MgO was used. Increasing the weight load percent of MgO to 70 wt.% decreased the catalyst surface area drastically to 17 m^2/g and therefore decreased the CH_4 and CO_2 conversions owing to the hindrance of reducing NiO by the robust interaction with the support, as shown by the H_2-TPR analysis. The 5Ni-MgO exhibited the lowest total hydrogen consumptions due to the formation of solid solution between NiO and MgO. The catalyst with 20wt.%-MgO displayed low weight loss of 11% during TGA analysis due to its low reactivity. While the optimum catalyst 5Ni-MG63 gave significant weight loss of 39% as a result of its high activity. The catalyst supported on unmodified Al_2O_3 gave the highest weight loss of 77%, which indicated the modification of the support with MgO addition assisted in reducing the carbon formation.

Supplementary Information The online version contains supplementary material available at https://doi.org/10.1007/s11164-023-05117-0.

Acknowledgements The authors would like to extend their sincere appreciation to the Researchers Supporting Project (number RSP2023R368), King Saud University, Riyadh, Saudi Arabia

Author contributions YAB, AAF and AAI contributed to the analysis of preparation of catalysts and writing; AB, JAD and AHF contributed to the analysis, writing, reviewing and editing; FSA, AIA and AEA contributed to the investigation; methodology, conceptualization and analysis. All authors have read and agreed to the published version of the manuscript.

Funding By Researchers Supporting Project (number RSP2023R368), King Saud University, Riyadh, Saudi Arabia.

Data availability All relevant data are within the manuscript and available from the corresponding author upon request.

Declarations

Conflict of interest The authors declare that they have no competing interests.

Ethical approval Not applicable.

References

1. D.A. Slade, A.M. Duncan, K.J. Nordheden, S.M. Stagg-Williams, Green Chem. **9**, 577 (2007)
2. Z. Hao, Q. Zhu, Z. Jiang, H. Li, Powder Technol. **183**, 46 (2008)
3. A.S.A. Al-Fatish, A.A. Ibrahim, A.H. Fakeeha, M.A. Soliman, M.R.H. Siddiqui, A.E. Abasaeed, Appl. Catal. A **364**, 150 (2009)
4. S. Vasileiadis, Z. Ziaka-Vasileiadou, Chem. Eng. Sci. **59**, 4853 (2004)
5. H. Sun, H. Wang, J. Zhang, Appl. Catal. B Environ. **73**, 158 (2007)
6. A.P.E. York, T.C. Xiao, M.L.H. Green, J.B. Claridge, Catal. Rev. Sci. Eng. **49**, 511 (2007)
7. J. Ma, N. Sun, X. Zhang, N. Zhao, F. Xiao, W. Wei, Y. Sun, Catal. Today **148**, 221 (2009)
8. A.S. Al-Fatesh, Int. J. Hydrog. Energy **42**, 18805 (2017)
9. G.C. de Araujo, S.M. de Lima, J.M. Assaf, M.A. Peña, J.L.G. Fierro, M. do Carmo Rangel, Catal. Today **133**, 129 (2008)
10. M. Akri, S. Zhao, X. Li, K. Zang, A.F. Lee, M.A. Isaacs, W. Xi, Y. Gangarajula, J. Luo, Y. Ren, Y.T. Cui, L. Li, Y. Su, X. Pan, W. Wen, Y. Pan, K. Wilson, L. Li, B. Qiao, H. Ishii, Y.F. Liao, A. Wang, X. Wang, T. Zhang, Nat. Commun. **10**, 5181 (2019)
11. A.S. Al-Fatesh, Y. Arafat, H. Atia, A.A. Ibrahim, Q.L.M. Ha, M. Schneider, M.A.H. . M-Pohl, Fakeeha, J. CO2 Util. **21**, 395 (2017)
12. I.R. Azevedo, A.A.A. da Silva, Y.T. Xing, R.C. Rabelo-Neto, N.T.J. Luchters, J.C.Q. Fletcher, F.B. Noronha, L.V. Mattos, Int. J. Hydrog. Energy **47**, 15624 (2022)
13. J.C.S.. Araújo, L.F. Oton, B. Bessa, A.B.S. Neto, A.C. Oliveira, R. Lang, L. Otubo, J.M.C. Bueno, Fuel **254**, 115681 (2019)
14. G. Ruan, Z. Zhang, M. Yin.-Rare Metals, **30**, 506 (2011)
15. S. Therdthianwong, C. Siangchin, A. Therdthianwong, Fuel Process. Technol. **89**, 160 (2008)
16. F. Pompeo, N.N. Nichio, M.M.V.M. Souza, D.V. Cesar, O.A. Ferretti, M. Schmal, Appl. Catal. A **316**, 175 (2007)
17. S. Moogi, C.H. Ko, G.H. Rhee, B.H. Jeon, M. Khan, Y.K. Park, Chem. Eng. J. **437**, 135348 (2022)
18. J.F. Da Costa-Serra, A. Chica, Int. J. Hydrog. Energy **36**, 3862 (2011)
19. S.O. Kasim, A.S. Al-Fatesh, A.A. Ibrahim, R. Kumar, A.E. Abasaeed, A.H. Fakeeha, Int. J. Hydrog. Energy **45**, 33343 (2020)
20. S. Afzal, D. Sengupta, A. Sarkar, M. El-Halwagi, N. Elbashir, ACS Sustain. Chem. Eng. **6**, 7532 (2018)
21. A.S.A. Al-Fatesh, A.A. Ibrahim, A.H. Fakeeha, A.E. Abasaeed, M.R.H. Siddiqui, J. Ind. Eng. Chem. **17**, 479 (2011)
22. O. Dewa, D. Makoka, O.A. Ayo-Yusuf, Int. J. Disaster Risk Sci. **12**, 673 (2021)
23. J. Huo, J. Jing, W. Li, Int. J. Hydrog. Energy **39**, 21015 (2014)
24. A. Kumari, R. Gupta, S. Tanwar, S. Tyagi, N. Kumar, IEEE Netw. **34**, 299 (2020)
25. L. Xu, H. Song, L. Chou, Appl. Catal. B Environ. **108**, 177 (2011)
26. C.M.R. Almeida, M.E. Ghica, L. Durães, Adv. Colloid Interface Sci. **282**, 102189 (2020)
27. T. Horiuchi, K. Sakuma, T. Fukui, Y. Kubo, T. Osaki, T. Mori, Appl. Catal. A **144**, 111 (1996)
28. Y.H. Hu, E. Ruckenstein, Catal. Lett. **43**, 71 (1997)
29. B.Q. Xu, J.M. Wei, Y.T. Yu, J.L. Li, Q.M. Zhu, Top. Catal. **22**, 77 (2003)
30. S. Wang, G.Q.M. Lu, Appl. Catal. B Environ. **16**, 269 (1998)
31. N.D. Charisiou, G. Siakavelas, L. Tzounis, V. Sebastian, A. Monzon, M.A. Baker, S.J. Hinder, K. Polychronopoulou, I.V. Yentekakis, M.A. Goula, Int J. Hydrog. Energy **43**, 18955 (2018)
32. A. Siahvashi, A.A. Adesina, Int J. Hydrog. Energy **43**, 17195 (2018)
33. T. Cui, Q. Chen, Y. Zhang, B. Nie, B. Yang, Appl. Surf. Sci. **599**, 154002 (2022)
34. S.Y. Foo, C.K. Cheng, T.-H. Nguyen, E.M. Kennedy, B.Z. Dlugogorski, A.A. Adesina, Catal. Commun. **26**, 183 (2012)
35. G.I. Siakavelas, N.D. Charisiou, A. AlKhoori, S. AlKhoori, V. Sebastian, S.J. Hinder, M.A. Baker, I.V. Yentekakis, K. Polychronopoulou, M.A. Goula, J. CO2 Util. **51**, 101618 (2021)
36. K. Fujimoto, K. Tomishige, O. Yamazaki, Y. Chen, X.H. Li, Res. Chem. Intermed. **24**, 259 (1998)
37. B. Jin, S. Li, X. Liang, Fuel **284**, 119082 (2021)
38. M. Jafarbegloo, A. Tarlani, A.W. Mesbah, S. Sahebdelfar, J. Nat. Gas Sci. Eng. **27**, 1165 (2015)

Authors and Affiliations

Yousef A. Al-Baqmaa[1] · Ahmed S. Al-Fatesh[1] · Ahmed A. Ibrahim[1] · Abdulaziz A. Bagabas[2] · Fahad S. Almubadde[1] · Abdulaziz I. Alromaeh[2] · Jehad K. Abu-Dahrieh[3] · Ahmed E. Abasaeed[1] · Anis H. Fakeeha[1]

✉ Ahmed S. Al-Fatesh
aalfatesh@ksu.edu.sa

✉ Abdulaziz A. Bagabas
abagabas@hotmail.com

✉ Jehad K. Abu-Dahrieh
j.abudahrieh@qub.ac.uk

Yousef A. Al-Baqmaa
youssef201629@gmail.com

Ahmed A. Ibrahim
aidid@ksu.edu.sa

Fahad S. Almubadde
falmubaddel@ksu.edu.sa

Abdulaziz I. Alromaeh
aalrumayh@kacst.edu.sa

Ahmed E. Abasaeed
abasaeed@ksu.edu.sa

Anis H. Fakeeha
anishf@ksu.edu.sa

[1] Chemical Engineering Department, College of Engineering, King Saud University, P.O. Box 800, Riyadh 11421, Saudi Arabia

[2] Executive Office, King Abdulaziz City for Science and Technology (KACST), P. O. Box 6086, Riyadh 11442, Saudi Arabia

[3] School of Chemistry and Chemical Engineering, Queen's University Belfast, Belfast BT9 5AG, Northern Ireland, UK